Frozen Impacted Drop: From Fragmentation to Hierarchical Crack Patterns

Elisabeth Ghabache, Christophe Josserand, and Thomas Séon
Sorbonne Universités, UPMC Université Paris 06, UMR 7190, Institut Jean Le Rond d'Alembert, F-75005 Paris, France and CNRS, UMR 7190, Institut Jean Le Rond d'Alembert, F-75005 Paris, France
(Received 5 May 2016; published 9 August 2016)

We investigate experimentally the quenching of a liquid pancake, obtained through the impact of a water drop on a cold solid substrate (0 °C to −60 °C). We show that, below a certain substrate temperature, fractures appear on the frozen pancake and the crack patterns change from a 2D fragmentation regime to a hierarchical fracture regime as the thermal shock increases. The different regimes are discussed and the transition temperatures are estimated through classical fracture scaling arguments. Finally, a phase diagram presents how these regimes can be controlled by the drop impact parameters.

DOI: 10.1103/PhysRevLett.117.074501

When molten glass drips into cold water, the outside cools—and shrinks—faster than the inside, creating pent-up tension in the so-called Prince Rupert's drop, known since before 1625 to have very striking mechanical properties [1,2]. Indeed, while the drop's head stays impervious to even the strongest blows, flick the tail and the whole drop shatters in a myriad of small pieces, in less than a millisecond. In the same way, fragmentation is in fact present in many physical processes, from jet atomization to bubble bursting in fluids [3–5], from spaghetti breaking [6] to popping balloons [7] or broken windows in solids [8,9]. It is related to diverse applications such as comminution [10], shell case bursting [11,12], ash generation during eruption [13,14], cooling lava [15], or meteoric cratering [16], for instance.

Fragmentation is thus a sudden process, where the whole considered domain divides extremely rapidly. At least as ubiquitous, there exists a completely different crack morphology where a space-dividing pattern shows a strong hierarchy of slower fractures [17]. Fractures develop successively, and each new fracture joins older fractures at a typical angle close to 90° [18,19]. Such patterns are usually observed when the shrinking of a material layer is frustrated by its deposition on a nonshrinking substrate, such as drying-induced cracks in mud [20,21], coffee [22], colloidal silicas [23], industrial coating [24], or artistic painting [25].

In this Letter, we investigate experimentally the quenching of a liquid pancake (Fig. 1) that is obtained through the impact of a water drop on a cold solid substrate. We show for the first time that, as a function of the substrate temperature, the crack patterns produced by the thermal shock change from a 2D fragmentation regime to a hierarchical fracture regime [Fig. 2(a)].

The experimental setup consists of releasing a drop of water, with a diameter $D_0 = 3.9$ mm, on a steel substrate, so as to form a liquid pancake of radius R and typical thickness h_0 (Fig. 1). At room temperature, both are determined by the impact parameters (see, e.g., Ref. [26] for the exact expression). The impact velocity is close to the free fall one: $U_0 \sim \sqrt{gH}$, where H is the falling height. Throughout most of the Letter, the falling height will be kept constant at $H = 36$ cm. The subsequent pancake radius is $R \simeq 8$ mm, from which pancake thickness can be estimated by balancing the volume of the drop with that of the cylindrical pancake $h_0 = D_0^3/6R^2 \simeq 150$ μm. The temperature of the substrate T_s is homogeneous, measured by contact thermometers at different locations, and typically varies from the water freezing temperature, 0 °C, to −60 °C. The desired temperature is reached by plunging a large cube of stainless steel (10^3 cm^3) into liquid nitrogen. The whole experiment is made into a glove box where the humidity is controlled in order to avoid frost formation. Because of the small experiment time (max ∼1 s), we can keep in mind that the substrate remains at constant temperature during the dynamics. The drop dynamics is visualized using a high-speed camera recording the spreading from the top.

Figures 2(b) and 2(c) present time sequences for different substrate temperatures, −31 °C and −60 °C, respectively. In both impact sequences, the drop spreads on the substrate until it reaches its maximum diameter, captured in the second image. During this phase, the droplet remains liquid but a thin layer of ice forms upon contact with the substrate.

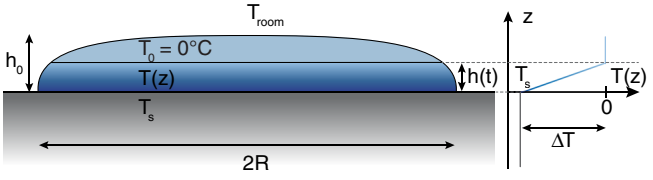

FIG. 1. Scheme of the frozen pancake obtained after a liquid drop impacted a cold substrate. The pancake has a radius R and a typical thickness h_0. The substrate, at a temperature T_s, cools the pancake, so that a layer of thickness $h(t)$ is frozen, above which the liquid is at the freezing temperature T_0.

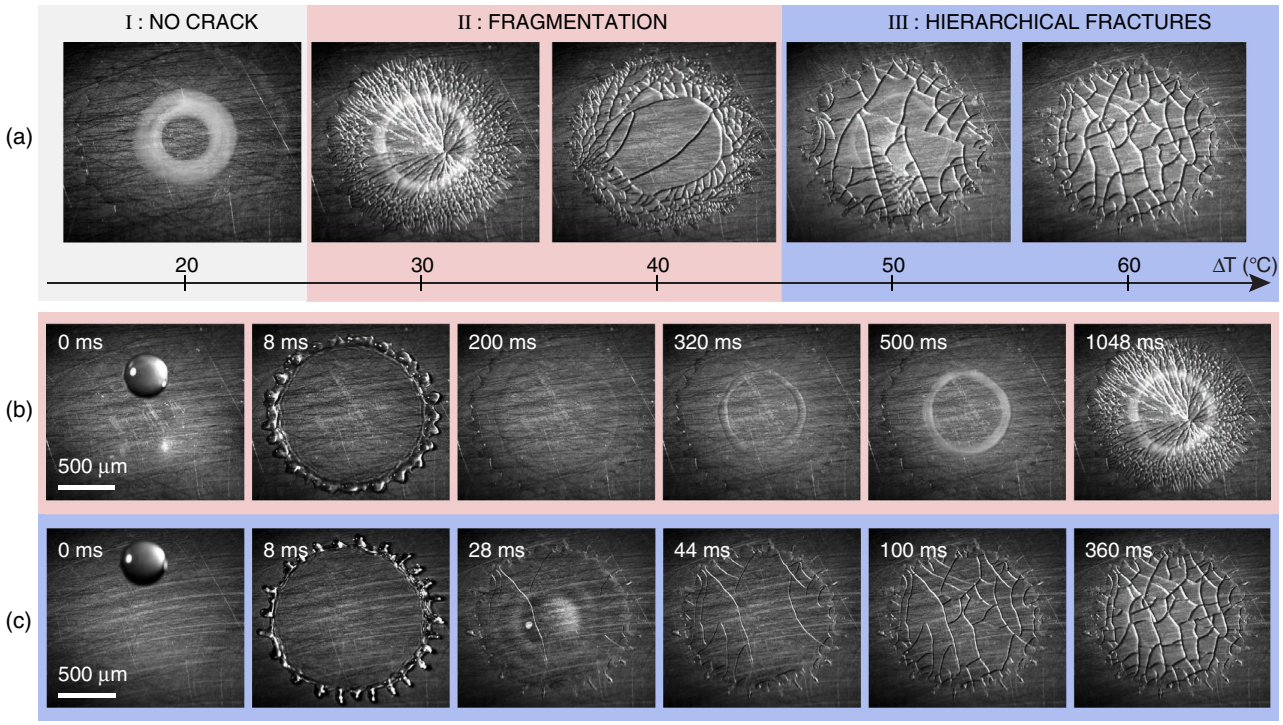

FIG. 2. (a) Frieze presenting snapshots of the frozen pancakes formed after a water drop impacted, from a falling height $H = 36$ cm, a cold substrate at various temperatures, $T_s = -20.0\,°C$, $-31.1\,°C$, $-41.2\,°C$, $-50.3\,°C$, and $-59.6\,°C$ from left to right (with $\Delta T = -T_s$). Depending on ΔT, the frozen pancake presents different crack patterns that can be gathered into three different regimes: (I) no cracks, (II) fragmentation regime, (III) hierarchical fracture regime. The transition temperatures are $\Delta T_{\text{I-II}}^{(\text{exp})} \sim 27\,°C$ and $\Delta T_{\text{II-III}}^{(\text{exp})} \sim 42\,°C$. (b) Sequence showing the drop impact and solidification dynamics preceding the fracture pattern observed on the second image of (a): $T_s = -31.1\,°C$. (c) Sequence preceding the fracture pattern observed on the fifth image of (a): $T_s = -59.6\,°C$. On these two sequences, the time and the scale bar are on the images.

In contrast to the situation at room temperature [26], almost no retraction of the drop is further observed since it is pinned on the solid substrate, most probably by this ice layer. Instead, capillary waves propagate on the spread droplet, which now has the shape of a pancake. In the meantime, the solidification of the drop occurs, observed in Fig. 2(b) through a front that develops radially from the pancake edge towards its center, forming eventually a doughnut that solidifies ($t \sim 500$ ms) because of the complex dynamics of the solidification front [27]. After that point [$t \sim 500$ ms in Fig. 2(b)], the whole pancake is frozen and keeps cooling. It is therefore shrinking, but the adhesion to the solid substrate limits this ice contraction. This frustration causes mechanical tensions that are suddenly relaxed by the formation of a pattern of fractures. This remarkable dynamics, called fragmentation, is a 2D equivalent to the Prince Rupert's drop shattering described in the Introduction. This solid fragmentation seems to propagate radially from a nucleation point. Experimental estimation gives a high front propagation velocity, typically between 800 and 1000 m s^{-1}, which is a fraction of the Rayleigh wave speed.

Figure 2(c) presents the same drop impact experiment, but on an even colder substrate ($-46\,°C$). In this case, shortly after the drop has pinned, while ripples are still visible, first fractures are observed on a growing ice layer ($t \sim 28$ ms). Then more cracks propagate, hierarchically, by a successive division of the frozen drop. The crack pattern here is typical of hierarchical fractures [17], with the younger crack joining the older one at an angle close to 90°. The domains are larger—and consequently less numerous—than in the fragmentation regime. Note that, if this particular cracking dynamics is very similar to what is observed in the case of desiccation [22], the time scales are much shorter.

To summarize the qualitative description of our experiment, the main different patterns are shown in Fig. 2(a) as a function of the temperature difference $\Delta T = T_0 - T_s$, where T_s is the substrate temperature and $T_0 = 0\,°C$ is the water freezing temperature. They are gathered in three different regimes: (I) At low ΔT, the solid pancake remains smooth—no cracks are present. (II) The fragmentation regime, at intermediate ΔT—the cracks appear suddenly from a nucleation point. (III) The hierarchical regime, at high ΔT—the cracks are formed step by step.

The two sequences described above, Figs. 2(b) and 2(c), belong to the beginning of regime II and the end of regime III, respectively. We observe that, close to the transition

between the regimes, intermediate cases appear, with fragmentation only on the edge of the pancake or the mix between the fragmentation and hierarchical fractures. It is also worth emphasizing that while the fragmentation occurs after the whole pancake has solidified, the hierarchical cracks are usually formed during the solidification phase: if the bottom part of the pancake is solid, a liquid layer is still present on the top. Finally, this experiment provides, to our knowledge, the first example where it is possible to pass continuously from a fragmentation to a hierarchical regime using a simple control parameter. Thermal shock in ceramic [28,29] might display comparable behavior, but this has not been observed so far.

These different regimes can be understood using classical fracture arguments [30]: indeed, since the freezing of the liquid is at 0 °C, the new solid is submitted to a rapid thermal contraction since the substrate temperature is smaller. If the ensuing deformation energy is high enough, fractures can appear in the frozen pancake. This mechanism can be quantified using energy balance [31,32]: we assume a linear isotropic elastic behavior of ice, with a Young's modulus $E = 9.33$ GPa. Its thermal contraction induces a deformation tensor field $\varepsilon_{\text{th}}(\mathbf{x}, t) = \alpha\delta T\mathbf{I}$, where $\alpha = 5.3 \times 10^{-5}$ K^{-1} is the ice thermal expansion coefficient taken constant here [33], $\mathbf{I}$ is the identity tensor, and $\delta T = T_0 - T(\mathbf{x}, t)$, with $T(\mathbf{x}, t)$ being the local time-dependent temperature in the ice domain. The density of the elastic energy induced by this thermal contraction reads, therefore, $\mathcal{E} = \frac{3}{2}E\alpha^2\delta T^2$.

A fracture in a brittle material consists of the formation of a new interface, associated with an energy per unit surface, the so-called Griffith energy, $G_c \simeq 1$ kg s^{-2} [34]. Balancing the elastic energy due to the thermal contraction of a cubic ice of length L_c, with homogeneous temperature T_s, $3E(\alpha\Delta T)^2L_c^3/2$, with the energy of a crack breaking the cube in the two part $2G_cL_c^2$, leads to the introduction of the Griffith length:

$$L_c = \frac{4G_c}{3E\alpha^2\Delta T^2}. \tag{1}$$

Above this typical length, breaking the shrunk solid becomes energetically favorable.

In our system, three regimes can therefore be identified in the crack formation, depending on the ratio between the Griffith length L_c and the typical height h_0 of the liquid pancake [35]. If $h_0 \ll L_c$, no crack formation is expected from the thermal shock, this first regime is observed in the first image of Fig. 2(a). On the other hand, for $h_0 \gg L_c$, one expects the cracks to appear before the whole solidification of the pancake, when a solid ice layer of thickness of the order of L_c is formed. This is the behavior observed in Fig. 2(c) and, therefore, corresponding to regime III. In between, for $h_0 \sim L_c$, one expects the cracks to be formed when the whole pancake is solid, and we identify the latter behavior with regime II [Fig. 2(b)], where the frozen pancake fragments into a myriad of small pieces of a typical size h_0 [17].

Let us start by estimating the appearance temperature of the first cracks at the frontier between regimes I and II, $\Delta T_{\text{I-II}}$. Energy balance requires the total elastic energy in the frozen pancake to be greater than the surface energy of all of the fractures, namely,

$$\frac{3}{2}E\alpha^2\Delta T^2\pi R^2h_0 \geq 4\frac{\pi R^2}{h_0^2}G_ch_0^2,$$

where the ratio $\pi R^2/h_0^2$ is the number of pieces of the typical size h_0 formed by the fragmentation. It leads to the relation

$$\Delta T^2 \geq \Delta T_{\text{I-II}}^2 = \frac{8G_c}{3E\alpha^2h_0}. \tag{2}$$

For $\Delta T > \Delta T_{\text{I-II}}$, the cracks are energetically favorable, while no cracks should be observed otherwise. At this transition temperature, the pancake thickness is then found to be twice the Griffith length. Taking the values of E, G_c, and h_0 given above leads to $\Delta T_{\text{I-II}} \sim 26$ °C, which is in excellent agreement with the experimental transition temperature to fragmentation $\Delta T_{\text{I-II}}^{(\text{exp})} \sim 27$ °C (Fig. 2).

On the other hand, when $h_0 \gg L_c$, fractures can form before the full solidification of the liquid pancake, and we identify there regime III, where the cracks appear step by step. In this case, the solid layer of the thickness $h(t)$ grows with time as the pancake freezes (see Fig. 1), while the liquid temperature can be considered constant and equal to T_0 because of the high contrast between the water and air thermal conductivities. The diffusive heat flux through this solid layer, $Q = -\lambda\partial_z T$, is then balanced, at the solidification front, by the solidification rate $-\rho_s L\dot{h}(t)$. Here, $L = 333.5$ kJ kg^{-1} is the ice-water latent heat per unit mass, $\rho_s = 920$ kg m^{-3} the density of the ice, and $\lambda = 2.4$ W m^{-1} K^{-1} its thermal conductivity [33]. This gives a time scale for the solidification process, $\tau_s = \rho_s Lh^2/\lambda\Delta T$. Comparing the latter to the time scale of heat diffusion $\tau_d = h^2/D$ leads to the Stefan number:

$$\text{St} = \frac{C_p\Delta T}{L} = \frac{\tau_d}{\tau_s},$$

where $D = \lambda/\rho_s C_p = 1.3 \times 10^{-6}$ m^2 s^{-1} is the heat diffusion coefficient of the ice. In our experiments, the Stefan number is always smaller than one, indicating that the diffusion process is always faster than the solidification dynamics. Therefore, we can consider that the temperature field in the ice layer is in a quasistationary regime, obeying the stationary diffusion equation. Taking a simple horizontal ice layer of height $h(t)$, it reads $\partial_{zz}T = 0$, with the

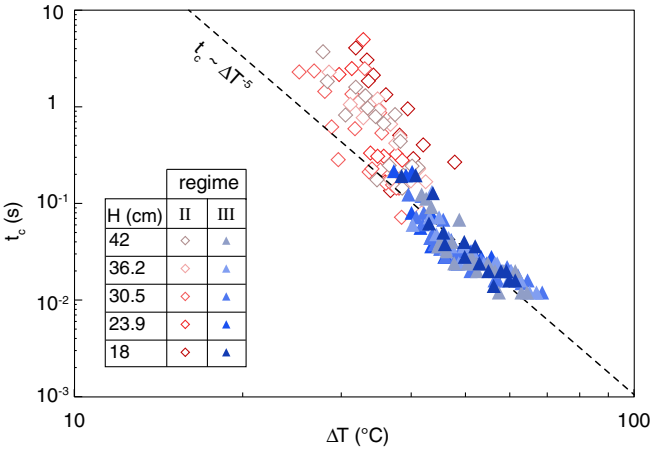

FIG. 3. Appearance time of the first crack, t_c, plotted as a function of $\Delta T = T_0 - T_s = -T_s$, with T_s being the substrate temperature, for five different falling heights of the impacting drop. t_c is determined considering the initial time when the drop reached its maximum spreading diameter after impact. The open diamonds correspond to the fragmentation regime (II), while the closed triangles correspond to the hierarchical fracture regime (III). The dashed line, representing $t_c \propto \Delta T^{-5}$, follows reasonably well the points in regime III.

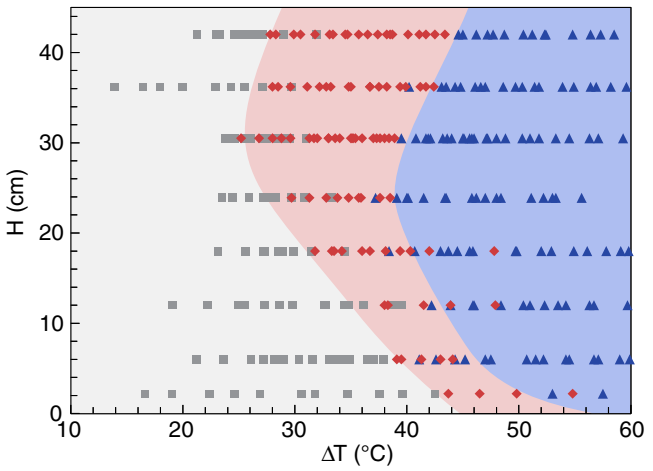

FIG. 4. Phase diagram for the cracks pattern as the substrate temperature ($-\Delta T$) and the drop impact velocity (here noted by H, the height of the drop fall) vary. The three regimes observed are represented with the same symbols and the same color as in Fig. 2: white squares for regime I, red diamonds for regime II, and blue triangles for regime III.

boundary conditions $T(0,t) = T_s$ and $T(h(t),t) = T_0$ since the temperature at the solidification front $z = h(t)$ is the freezing temperature. This leads to the linear temperature field:

$$T(z,t) = T_s + \Delta T \frac{z}{h(t)}. \tag{3}$$

Now, balancing the time-dependent diffusive heat flux through the ice, $Q = -\lambda \partial_z T = -\lambda \Delta T / h(t)$, with the solidification rate, $-\rho_s L \dot{h}(t)$, gives the following time evolution for the ice layer:

$$h^2(t) = \frac{2\lambda \Delta T}{\rho_s L} t = 2\mathrm{St} D t,$$

with $h(0) = 0$. Considering that the formation of the first crack happens when $h(t_c) \propto L_c$ [Eq. (1)], it gives for the time of cracks appearance in regime III

$$t_c \propto \frac{8\rho_s L G_c^2}{9\lambda E^2 \alpha^4 \Delta T^5}. \tag{4}$$

This first crack time t_c has been measured for all of our experiments, varying both the impact velocity and the substrate temperature, and is shown in Fig. 3. The closed triangles correspond to the appearance of the first crack in regime III, in reasonable agreement with the ΔT^{-5} variation predicted by the relation (4), plotted with a dashed line. This confirms our model where quasistationary heat diffusion in the ice layer drives the solidification rate, and the first crack appears when the thickness of the ice layer is close to the Griffith length. On the contrary, the open diamonds corresponding to the fragmentation time in regime II do not follow the same scaling since the solidification dynamics and the temperature fields in the solid are different.

Finally, the transition between regimes II and III is expected when $h_0 \sim L_c$. Then the elastic energy in the ice block has to be estimated at the time when the solidification ends; namely, when $h(t) = h_0$. Integrating the elastic energy density $\mathcal{E}$ on the pancake volume with the corresponding temperature field [Eq. (3)] yields

$$\frac{3E\alpha^2}{2} \Delta T_{\mathrm{II-III}}^2 \pi R^2 \int_0^{h_0} \left(1 - \frac{z}{h_0}\right)^2 dz = \frac{E\alpha^2}{2} \Delta T_{\mathrm{II-III}}^2 \pi R^2 h_0.$$

Balancing this energy with the minimal elastic energy needed to fragment ($\frac{3}{2} E\alpha^2 \Delta T_{\mathrm{I-II}}^2 \pi R^2 h_0$) allows us to obtain the transition temperature $\Delta T_{\mathrm{II-III}}$ separating the two fracture regimes,

$$\Delta T_{\mathrm{II-III}} = \sqrt{3} \Delta T_{\mathrm{I-II}}. \tag{5}$$

Taking $\Delta T_{\mathrm{I-II}} \sim 26°$ computed above leads to $\Delta T_{\mathrm{II-III}} \sim 45°$, which is in very good agreement with the experimental transition temperature $T_{\mathrm{II-III}}^{(\mathrm{exp})} = 42°$. Note that this gives a pancake thickness 6 times larger than the Griffith length at the transition.

Finally, only one falling height H has been considered for the drop so far, which signifies that the shape of the pancake has been kept almost constant. However, the drop impact enables control of the pancake aspect ratio and further on of the crack patterns of thin structures. Indeed, by

varying the impact parameters and the substrate temperature, our experimental setup allows us to span a large range of spreading dynamics, leading to a broad variety of frozen drop shapes [26,36,37]. Figure 4 displays the phase diagram as both H and ΔT vary, where the three main domains of Fig. 2 are retained, proving their universality. However, we observe that the transition temperatures vary nonmonotonically with the drop falling height: since increasing H decreases the pancake thickness (h_0), we would expect the transition temperatures $\Delta T_{\text{I-II}} \propto h_0^{-1/2}$ [Eq. (2)] and $\Delta T_{\text{II-III}} = \sqrt{3}\Delta T_{\text{I-II}}$ [Eq. (5)] to increase with H, which is only compatible in our experiment for H's greater than 25–30 cm. Below this height, the transition temperature decreases, which is not predicted by our model, probably because the frozen drop does not have the pancake cylindrical shape of Fig. 1 anymore.

In conclusion, in this Letter the different crack regimes of a frozen water pancake, shrunk by cooling and pinned on a nonshrinking substrate, are investigated using classical fracture scaling arguments. By increasing the thermal shock, the pancake undergoes two regimes: from fragmentation to hierarchical fracture. The appearance temperature of both regimes are determined, along with the scaling of the first crack time in the hierarchical fracture regime. This original experiment, therefore, constitutes a model system enabling us to easily investigate a broad range of fracture mechanisms and to progress in the understanding of the multiphysics aspects of crack patterns due to thermal shocks.

[1] C. Merrett, *The Art of Glass* (Octavian Pulleyn, London, 1662).
[2] S. Chandrasekar and M. Chaudhri, Philos. Mag. B **70**, 1195 (1994).
[3] P. Marmottant and E. Villermaux, Phys. Fluids **16**, 2732 (2004).
[4] E. Villermaux, Annu. Rev. Fluid Mech. **39**, 419 (2007).
[5] H. Lhuissier and E. Villermaux, J. Fluid Mech. **696**, 5 (2012).
[6] B. Audoly and S. Neukirch, Phys. Rev. Lett. **95**, 095505 (2005).
[7] S. Moulinet and M. Adda-Bedia, Phys. Rev. Lett. **115**, 184301 (2015).
[8] N. Vandenberghe, R. Vermorel, and E. Villermaux, Phys. Rev. Lett. **110**, 174302 (2013).
[9] N. Vandenberghe and E. Villermaux, Soft Matter **9**, 8162 (2013).
[10] J. Telling, E. Boyd, N. Bone, E. Jones, M. Tranter, J. MacFarlane, P. Martin, J. Wadham, G. Lamarche-Gagnon, M. Skidmore, T. Hamilton, E. Hill, M. Jackson, and D. Hodgson, Nat. Geosci. **8**, 851 (2015).
[11] N. Mott, Proc. R. Soc. A **189**, 300 (1947).
[12] F. Wittel, F. Kun, H. J. Herrmann, and B. H. Kröplin, Phys. Rev. Lett. **93**, 035504 (2004).
[13] P. Kokelaar, Bull. Volcanol. **48**, 275 (1986).
[14] E. J. Liu, K. V. Cashman, A. C. Rust, and S. R. Gislason, Geology **43**, 239 (2015).
[15] L. Goehring, L. Mahadevan, and S. W. Morris, Proc. Natl. Acad. Sci. U.S.A. **106**, 387 (2009).
[16] A. Sagy, J. Fineberg, and Z. Reches, J. Geophys. Res. **109**, B10209 (2004).
[17] S. Bohn, L. Pauchard, and Y. Couder, Phys. Rev. E **71**, 046214 (2005).
[18] K. A. Shorlin, J. R. de Bruyn, M. Graham, and S. W. Morris, Phys. Rev. E **61**, 6950 (2000).
[19] V. Lazarus and L. Pauchard, Soft Matter **7**, 2552 (2011).
[20] E. Kindle, J. Geol. **25**, 135 (1917).
[21] G. Korvin, Pure Appl. Geophys. **131**, 289 (1989).
[22] A. Groisman and E. Kaplan, Europhys. Lett. **25**, 415 (1994).
[23] L. Pauchard, F. Parisse, and C. Allain, Phys. Rev. E **59**, 3737 (1999).
[24] P. Xu, A. Mujumdar, and B. Yu, Drying Technol. **27**, 636 (2009).
[25] L. Pauchard, V. Lazarus, B. Abou, K. Sekimoto, G. Aitken, and C. Lahanier, Reflets Phys. **3**, 5 (2007).
[26] C. Josserand and S. Thoroddsen, Annu. Rev. Fluid Mech. **48**, 365 (2016).
[27] A. G. Marín, O. R. Enríquez, P. Brunet, P. Colinet, and J. Snoeijer, Phys. Rev. Lett. **113**, 054301 (2014).
[28] W. Korneta, S. K. Mendiratta, and J. Menteiro, Phys. Rev. E **57**, 3142 (1998).
[29] S. Lahlil, W. Li, and J. M. Xu, Old Potter's Almanack **18**, 1 (2013).
[30] L. Freund, *Dynamic Fracture Mechanics* (Cambridge University Press, Cambridge, England, 1990).
[31] M. Adda-Bedia, M. Ben Amar, and Y. Pomeau, Phys. Rev. E **54**, 5774 (1996).
[32] B. Bourdin, J.-J. Marigo, C. Maurini, and P. Sicsic, Phys. Rev. Lett. **112**, 014301 (2014).
[33] V. F. Petrenko and R. W. Whitworth, *Physics of Ice* (Clarendon Press, Oxford, 1999).
[34] E. M. Schulson and P. Duval, *Creep and Fracture of Ice* (Cambridge University Press, Cambridge, England, 2009).
[35] G. Gauthier, V. Lazarus, and L. Pauchard, Europhys. Lett. **89**, 26002 (2010).
[36] A. L. Yarin, Annu. Rev. Fluid Mech. **38**, 159 (2006).
[37] J. Eggers, M. Fontelos, C. Josserand, and S. Zaleski, Phys. Fluids **22**, 062101 (2010).